DETERMINATION OF THE GROUND MOTION ORBIT AMPLIFICATION FACTORS DEPENDENCE ON THE FREQUENCY FOR THE APS UPGRADE STORAGE RING*

V. Sajaev, C. Preissner, ANL, Argonne, IL 60439, USA

Abstract

The Advanced Photon Source (APS) is pursuing an upgrade to the storage ring that will provide electron beams with extremely low emittance. To allow users to take advantage of this small beam size, the beam orbit has to be kept stable to within a fraction of the beam size, which translates to a sub-micron orbit stability requirement. Ground motion significantly contributes to the overall expected beam motion, especially at lower frequencies where the ground motion has larger amplitudes. At the same time, the lattice amplification factors reduce when the ground motion becomes coherent at low frequencies. In this paper, we will present simulations of dependence of the lattice amplification factor on the ground motion coherence length and show results of ground motion coherence measurements at APS. After uthat, we will determine the dependence of the lattice amplification factors on the ground motion frequency, which can be used to calculate the expected effect of the ground motion on orbit stability.

INTRODUCTION

The Advanced Photon Source (APS) is planning an upgrade to the storage ring that will provide electron beam with extremely low emittance. The new lattice is based on the hybrid seven-bend achromat concept [1] and utilizes reverse bends to achieve natural emittance of 42 pm·rad [2]. The lattice has very strong focusing elements. For example, maximum quadrupole strengths increase nearly five-fold compared to the present APS lattice. Since the effect on orbit stability of quadrupole vibration due to ground motion is proportional to the quadrupole strength, it is expected that ground vibration will have stronger effect on the orbit in the new machine. At the same time, the orbit stability requirements, which are defined as a fraction of the electron beam size, will be much more stringent, see Table 1. In this situation, carefully predicting the effect of the ground vibration on the orbit stability becomes ever more important.

Figure 1 shows measured Power Spectral Density (PSD) of the APS tunnel floor displacement. To cover a wider frequency range, the measurement was performed simultaneously using a seismometer and an accelerometer. The valid data range is 0.008−50 Hz for the seismometer and 10−100 for the accelerometer. As expected [3], the overall PSD dependence on frequency is approximately $1/f^n$, where n is close to 4. The measurement gives approximately 10 nm rms floor motion noise in the typical measurement

Table 1: Beam stability requirements at insertion device source points

Plane	AC rms Motion 0.01 − 1000 Hz		Long Term Drift 7 Days	
Horizontal	1.25 μm	0.25 μrad	1 μm	0.6 μrad
Vertical	0.4 μm	0.17 μrad	1 μm	0.5 μrad

band of 1−100 Hz, which compares favorably with the orbit stability requirements in Table 1. However, when the band is extended to 0.01−100 Hz, the rms noise jumps to 2 μm. Even in the presence of the perfect orbit correction, one might wonder if the orbit can be expected to have noise of 0.4 μm when the Beam Position Monitors (BPM) are moving with the floor at a 2 μm rms noise level.
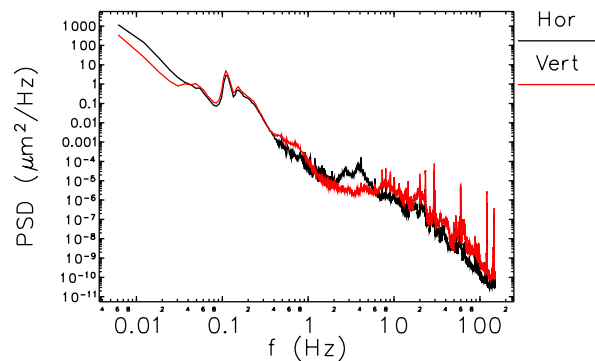

Figure 1: Power spectral density of the APS tunnel floor displacement. The wide frequency range is provided by combining measurements of seismometer in low-frequency range and accelerometer in high-frequency range.

Fortunately, the low-frequency ground motion has large wavelengths, and therefore the nearby magnets and BPMs move together. This should reduce the effect of the ground motion on the orbit, since for sufficiently low-frequency motion, the wavelength can exceed the dimensions of the storage ring. In this case, the entire storage ring would move together, which is equivalent to no motion at all. That is why it is important to understand the effect of the ground motion coherence on the orbit motion at low frequencies. In this paper, we will present ground motion coherence length measurements and describe calculations of the orbit amplification factors dependence on the coherence length. The coherence length concept should not work for diffusion-like

ground motion [4], but we believe that this type of motion has very little contribution above 0.01 Hz.

FLOOR MOTION COHERENCE LENGTH MEASUREMENT

The magnitude-squared coherence between two signals $x(n)$ and $y(n)$ is defined as

$$C_{xy}(\omega) = \frac{|P_{xy}(\omega)|^2}{P_{xx}(\omega)P_{yy}(\omega)},$$

where P_{xx} and P_{yy} are PSD of individual signals and P_{xy} is the cross-spectral density of the two signals [5]. Ground motion coherence length was measured in the APS tunnel in May 2017. Two identical seismometers REFTEK 151B-120 and a Data Physics vibration data acquisition system were used. Three axes of motion – transverse, vertical, and longitudinal with respect to the beam – were measured with each seismometer. For each measurement, 640 seconds of data were sampled at 1024 Hz. The specified valid frequency range of the seismometers is 0.008−50 Hz. The seismometers measure ground velocity, but the PSD of the ground displacement can be obtained by dividing the velocity PSD by $(2\pi f)^2$. As a first step, one needs to ensure that the motion measured by two seismometers placed next to each other shows a high level of coherence in a wide frequency range. Figure 2 shows the coherence of horizontal and vertical ground motion measured by two seismometers sitting next to each other. The motion is generally considered coherent when the coherence exceeds 0.8. One can see that two sensors show very good coherence between 0.1 and 20 Hz, the coherence above 20 Hz is reasonable up to 50 Hz (upper limit of the sensors' valid measurement range). One should also expect a high level of coherence for motion below 0.1 Hz, however, the measurements show decreasing coherence below 0.02 Hz. We attribute this to the device measurement noise.
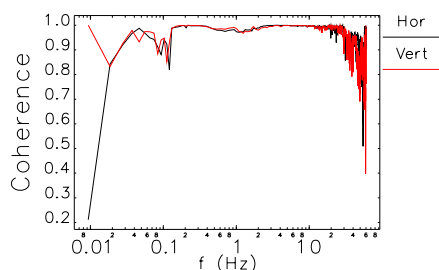

Figure 2: Coherence of horizontal and vertical measurements when two seismometers are located next to each other.

Having confirmed coherence of colocated devices, measurements were made as the seismometers were gradually moved apart. As seen in Fig. 3, the vertical motion becomes coherent below 1 Hz for distances at least up to 110 m (coherence above 0.8, red color on the plots). Horizontal coherence plot shows decreasing coherence at large distances due to

relative rotation of sensors, which were always oriented parallel to the beam. This resulted in 36° relative rotation of sensors at 110 m distance.
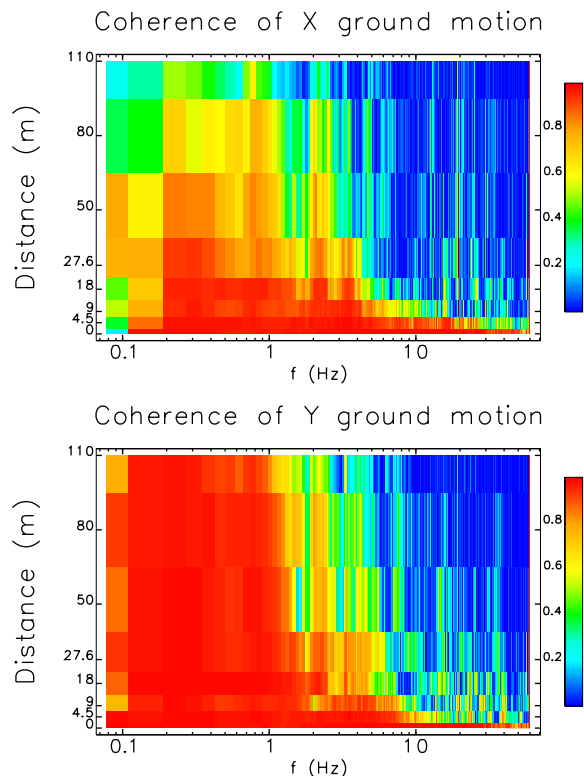

Figure 3: Coherence of ground motion as a function of distance between two sensors (top – horizontal motion, bottom -vertical motion). Horizontal and vertical axes are frequency and distance correspondingly, while color represents the coherence.

The coherence length dependence on frequency was obtained from the data above by determining for each distance the frequency where coherence exceeds 0.8, following which an exponential fit was used to approximate the frequency dependence, as shown in Fig. 4. Measurement at zero distance was ignored in the fit because it was likely limited by the seismometers upper range. The coherence lengths dependence on frequency can be approximated by

$$L_x \approx \frac{100}{f^{1.1}} \qquad \text{and} \qquad L_y \approx \frac{125}{f^{1.4}}. \qquad (1)$$

AMPLIFICATION FACTORS DEPENDENCE ON COHERENCE

Orbit amplification factors were calculated using static closed-orbit simulations by generating magnet displacements that have different correlation lengths and calculating the ratio of the resulting closed orbit and magnet displacement amplitude. The following procedure was used to generate random displacements with some correlation length: first, generate Gaussian-distributed random displacements

02 Photon Sources and Electron Accelerators

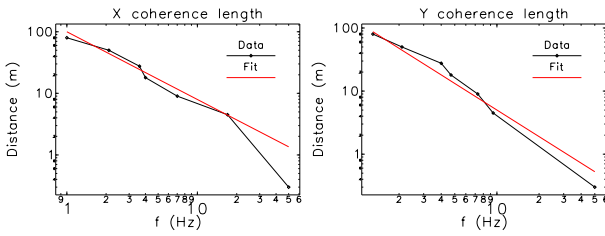**A05 Synchrotron Radiation Facilities**

Figure 4: Coherence length as a function of frequency, data and exponential fit. Left: horizontal data; right: vertical data.

of some amplitude for a grid of equally-spaced points; second, use a low-pass filter to "smooth" the random variations, where the cut-off frequency of the filter determines the correlation length; finally, scale the amplitude of the filtered displacements back to the initial amplitude (since filtering reduces the original amplitude of noise) and subtract average displacement, which is important for long correlation lengths. To filter the random displacements, the following program, which is part of the SDDS Toolkit [6], was used

sddsfdfilter -lowpass=f1=f_1,f2=f_2.

The transfer function of this command is 1 below f_1, 0 above f_2, and changes linearly between f_1 and f_2. When $f_1 = f_2 = f$, the filter above results in a sinc-like ringing at higher frequencies. To reduce this effect, we used $2f_1 = f_2/2 = f$. Figure 5 (left) shows comparison of the auto-correlation of two data sets filtered using $f_1 = f_2$ and $2f_1 = f_2/2$. If one defines correlation length as FWHM of the auto-correlation plot, then simulations show that the correlation length is approximately $1/(\sqrt{2}f)$.
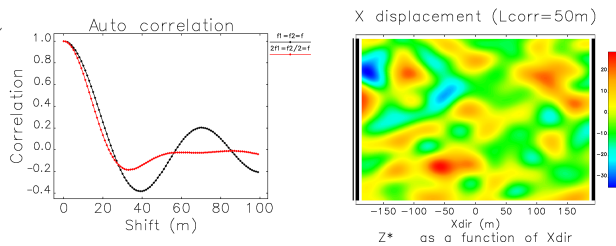

Figure 5: Left: auto-correlation of ground displacement generated by two different filters; the red line corresponds to the $2f_1 = f_2/2 = f$ filter used in the simulations. Right: Ground displacement: horizontal axis is x_{floor} and vertical axis is z_{floor}; the color is the displacement ΔX in nm.

To generate magnet displacements, the ground displacement was first generated in a square region completely containing the ring. We will call Cartesian coordinates describing this square "floor coordinates." As described above, random Gaussian-like displacements ΔX, ΔY, and ΔZ are generated and then "smoothed" separately along x_{floor} and z_{floor} axes. This results in a snap-shot of the ground displacement ΔX, ΔY, and ΔZ as function of x_{floor} and z_{floor}. Figure 5 (right) shows example of such displacement with correlation length of 50 m.

The displacements of magnets were calculated by sampling the ground displacement at the locations of the magnetic elements, which is done using bilinear interpolation based on the four nearest points on the square grid. After that, a straight line is fitted through all elements on one girder, and the elements are assigned new displacements according to this straight line. Displacements ΔX and ΔZ are then transformed from "floor" to "accelerator" coordinates by rotation; ΔY is unchanged.

The procedure described above was used to generate 100 sets of ground displacements for a set of different correlation lengths, and the closed orbit was calculated for every case using elegant [7]. For every correlation length, the orbit invariant $x^2/\beta + \beta x'^2$ taken at insertion device locations was averaged over 100 sets of ground displacements. The amplication factors were obtained by dividing the average orbit distortion invariant by the ground motion amplitude. As Fig. 6 (left) shows, the amplification vanishes around correlation length of 50 m.
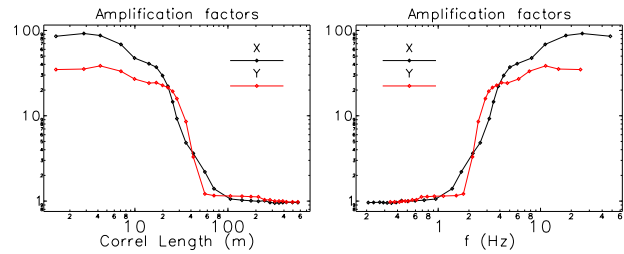

Figure 6: Horizontal and vertical orbit amplification factors. Left: as function of ground displacement correlation length; right: as a function of vibration frequency.

Now the data in Fig. 6 (left) and approximations (1) can be used to generate frequency dependence of the orbit amplification factors. Figure 6 (right) shows the results.

CONCLUSIONS

We have measured the coherence of ground motion in the APS tunnel as a function of distance between two points, finding that motion below 1 Hz is coherent for distances larger than 100 m. We then simulated static orbit amplification factors for different floor displacement correlation lengths. Combining these, we obtained orbit amplification factor dependence on ground vibration frequency. This dependence can be used to estimate rms orbit noise due to floor vibration.

REFERENCES

[1] L. Farvacque *et al.*, in *Proc. 2013 IPAC*, p. 79 (2013).

[2] M. Borland *et al.*, in *Proc. NAPAC 2016*, pp. 877–880 (2016).

[3] A. Sery *et al.*, *Phys Rev E*, 53:5323 (1996).

[4] V. Shiltsev. *Phys Rev ST Accel Beams*, 13:094801 (2010).

[5] J. S. Bendat *et al.*, "Random Data", Wiley-Interscience (1986).

[6] M. Borland *et al.*, User's Guide for SDDS Toolkit (2014), `https://ops.aps.anl.gov/oagSoftware.shtml`

[7] M. Borland, Advanced Photon Source report ANL/APS LS-287, (2000).